Peer-reviewed version available at J. Imaging 2018, 4, 108; doi:10.3390/jimaging4090108

Type of the Paper (Article)

Adaptive Multi-Scale Entropy Fusion De-hazing based on Fractional Order

Uche A. Nnolim*

Department of Electronic Engineering, University of Nigeria, Nsukka, Enugu, Nigeria; uche.nnolim@unn.edu.ng

* Correspondence: uche.nnolim@unn.edu.ng

Abstract: This paper describes a proposed fractional filter-based multi-scale underwater and hazy image enhancement algorithm. The proposed system combines a modified global contrast operator with fractional order-based multi-scale filters used to generate several images, which are fused based on entropy and standard deviation. The multi-scale-global enhancement technique enables fully adaptive and controlled colour correction and contrast enhancement without over exposure of highlights when processing hazy and underwater images. This in addition to illumination/reflectance estimation coupled with global and local contrast enhancement. The proposed algorithm is also compared with the most recent available state-of-the-art multi-scale fusion de-hazing algorithm. Experimental comparisons indicate that the proposed approach yields better edge and contrast enhancement results without halo effect, colour degradation and is faster and more adaptive than all other algorithms from the literature.

Keywords: Fractional order calculus-based multi-scale contrast operator; hybrid local-global contrast enhancement; underwater image enhancement processing; hazy image contrast enhancement; entropy guided fusion

1. Introduction

Hazy and underwater images share similar characteristics in terms of reduced visibility and low contrast due to the nature of image formation [1] [2]. Several single image-based enhancement and restoration models and algorithms have been proposed to solve this problem [1] [2]. However, they work with varying degrees of success at the cost of increased structural and computational complexity. Consequently, there are relatively few digital hardware realizations and reduced real-time prospects for such schemes due to high computational cost.

In this work we propose a fractional order-based algorithm for enhancement of hazy and underwater images. The algorithm utilizes an improved global contrast operator, which performs colour correction while a fractional order, multiscale spatial filter-based scheme performs localized enhancement. In the filter kernel is implemented using fractional calculus and combined with global contrast operators for further enhancement. Furthermore, the scheme is incorporated into a partial differential equation-based flow to further improve results and control over the enhancement processes. We then compare results with other algorithms from the literature and show that the proposed system is effective with the fastest execution time.

The paper is outlined as follows; the second section provides the background, motivation and key contributions of the proposed system. Section three presents the proposed algorithms for both underwater and hazy image enhancement in addition to solutions to problems and modifications. Section four presents and compares the results (obtained using the proposed system) to other algorithms from the literature. The fifth section explicitly compares the proposed approach against a recent algorithm from the literature, further strengthening the justification of the proposed scheme. The final section presents the conclusion.

Peer-reviewed version available at J. Imaging 2018, 4, 108; doi:10.3390/jimaging4090108

2. Materials and Methods

2.1 Underwater image processing algorithms

Underwater image processing algorithms can be classified as either restoration, enhancement or colour correction- and illumination normalization-based approaches [2] and range from medium to high computational and structural complexity. The restoration-based algorithms incorporate de-blurring and de-hazing processes using either Weiner [3] deconvolution or dark channel prior (DCP)-based techniques respectively [2]. Examples include algorithms by Galdran et al [4], Li et al [5], Li and Guo [6], Zhao et al [7], Chiang and Chen [8], Wen et al [9], Serikawa and Lu [10], Carlevaris-Bianco et al [11], Chiang et al [12], etc. Conversely, the enhancement-based algorithms do not employ any models derived from physical phenomena or prior image information [2]. They utilize statistical/histogram-based or logarithmic contrast enhancement/stretching and colour correction techniques in their formulation. Examples include works by Iqbal et al [13], Ghani and Isa [14], Fu et al [15], Gouinaud et al [16], Bazeille et al [17], Chambah et al [18], Torres-Mendez and Dudek [19], Ahlen et al [20] [21], Petit et al [22], Bianco et al [23], Prabhakar et al [24], Lu et al [25] and Li et al [5]. Recently, entropy and gradient optimized underwater image processing algorithms based on partial differential equations were developed [26] [27] and yielded effective and automated enhancement surpassing results from previous algorithms.

The illumination normalization-based algorithms attempt to resolve uneven lighting issues in the acquired underwater images scenes. The algorithms in this class include works by Prabhakar et al [24], Garcia et al [28], Rzhanov et al [29], Singh et al [30] and Fu et al [15].

2.2 Hazy image processing algorithms

Hazy image processing also deals with visibility restoration of image scenes degraded by weather conditions and can be multi- or single-image based solutions [31]. Furthermore, hazy image processing algorithms can also be classified as either restoration or enhancement-based schemes. In the restoration-based hazy image processing, the de-hazing process is based on the hazy image formation model [31]. The objective is therefore to obtain the de-hazed image from the input hazy image. The algorithms in this class include the popular DCP method by He et al [32], which has been adopted and modified in various forms and a review of several DCP-based methods can be found in [1].

Other schemes include works based on segmentation [33] [34] [35], fusion [36] [37], geometry [38], Weighted Least Squares [39], variational [40] [41] [37] [42] and regularization approaches [34] using sparse priors [43] and other boundary constraints [44], biological retina-based model [45] and multi-scale convolutional neural networks [46]. The enhancement-based hazy image processing method is based on directly obtaining the by-product of radiance scene recovery through visibility restoration by contrast enhancement/maximization. The algorithms in this category utilize contrast limited adaptive histogram equalization (CLAHE), histogram specification (HS) [47] and Retinex [48] [49] [50]. Additionally, some of these algorithms combine dark channel priors and transmission map extraction with contrast enhancement for refinement. However, consistently good results are not guaranteed as some images will depict colour fading/distortion and darkening of regions in addition to over-enhancement of sky/homogeneous regions. Thus some threshold and segmentation-based algorithms [33] [34] [35] [51] have been developed to solve the peculiar problems of these algorithms. Furthermore, recently developed algorithms using partial differential equations (PDEs) and gradient metric-based optimization were developed [52] [53] to avoid the usage of DCP-based stages and multiple (and manual adjustment of) parameters. Recently, an Artificial Multiple-Exposure Image Fusion (AMEF) de-hazing algorithm was proposed by Galdran [54], which represents the current state-of-the-art.

Physical methods depend on prior image information obtained by capturing the image scenes at different times under varying conditions using physical hardware/optical equipment such as cameras and lighting rigs [2]. They may also incorporate multi-image processing schemes for either hazy or underwater images. However, consistently good results are not assured due to the

unpredictable nature of weather and aquatic medium conditions. Also the cost of such hardware imaging systems is prohibitive and are usually not universally applicable. Such schemes are fully listed and described in work by Li et al [5]. Single-image-based software implementations offer the best outcome when factors such as cost, time, replicability and convenience are considered since they do not necessarily require prior knowledge of the environment or image acquisition process for operation [2] [5]. Thus, the scope of this work is limited to single-image-based enhancement of both hazy and underwater images.

The primary motivation for this work is to develop fast, practical and effective algorithms for underwater and hazy image enhancement that are amenable to hardware implementation for real-time operation.

2.3 Key contributions and features of proposed scheme

The key contributions and features of this work include:

- A modified global contrast enhancement and a multi-scale illumination/reflectance model-based algorithm using fractional order calculus-based kernels.
- Relatively low- complexity underwater image enhancement algorithm utilizing colour correction and contrast operators.
- Frequency-based approach to image de-hazing and underwater image enhancement using successive, simultaneous high frequency component augmentation and low frequency component reduction.
- Feasible hazy and underwater image enhancement algorithm for relatively easier hardware architecture implementation utilizing fractional order calculus-based filters.
- Avoidance of dark channel prior based stages and iterative schemes by utilizing combined multi-level convolution using fractional derivatives.

3 Proposed algorithms

Underwater image enhancement usually involves some colour correction/white balancing in addition to contrast enhancement process, usually a local/global operation. The first step to reducing the need for such involved local processing was to avoid the over-exposure of bright regions while enhancing the dark regions. Initial logarithmic solutions were ineffective and flattened the images in addition to fading colours. Thus, a new formulation for the global contrast operator had to be devised to achieve this objective. We present the modification and realization of the improved global contrast operator and spatial filter based system for processing underwater and hazy images. Furthermore, the simplified scheme using integer and fractional calculus is presented in the form of spatial masks based on the Grunwald-Letnikov definition [55].

3.1 Selection and modification of global contrast operator

Previously, extensive experiments where conducted (to determine effectiveness) on several contrast stretching algorithms [26]. Due to adjustable nature of the high and low values by adjusting the percentiles, the contrast stretching (CS) algorithm appeared to be much more versatile than the other algorithms. However, it works best for faded low-contrast images but not so well for underwater images since it does not perform adequate colour correction unless applied iteratively. Conversely some of the other algorithms were too harsh, had no effect or minimal impact on most underwater images, while others resulted in colour bleeding. The selected algorithms such as the piecewise linear transform (PWL) [56] and the gain offset correction (GOC) [57] were selected for incorporation into effective PDE -based formulations [26] [27]. This was because some underwater images responded better to GOC2 (due to its mainly colour correction ability) than to PWL (due to

Peer-reviewed version available at J. Imaging 2018, 4, 108; doi:10.3390/jimaging4090108

its generality) and vice versa. Thus, there is the need to develop a global contrast operator that would merge the advantages of both GOC2 and PWL while mitigating their weaknesses.

Since the linear contrast stretch (similar to the PWL and GOC) does not utilize any edge enhancement features or region-based methods, it does not enhance noisy edge artefacts. However, several of these contrast stretching algorithms lead to oversaturation of already bright regions of the image (whitening out/over-exposure). This is in addition to a thresholding effect when applied to images with bimodal histogram. The linear contrast can be applied to both greyscale and colour images with excellent results similar to the PWL. However, the PWL method also suffers from the thresholding of images when there are distinct regions of dark and light intensity, leading to whiting out of bright areas. This is because it truncates values at upper and lower limits to maximum and minimum possible pixel values in the image without taking into account pixels in those regions, the linear contrast stretch seeks to expand the range based on the surrounding pixels in the distribution.

Underwater image enhancement usually involves some colour correction/white balancing in addition to contrast enhancement process, which is usually a local/global operation. The GOC2 algorithm adequately processed underwater images, which required mild colour correction and contrast enhancement and thus avoided overexposure of highlights unlike most other tested contrast enhancement algorithms [26]. This necessitated the incorporation of a local contrast operator such as the CLAHE, which though effective, further added to the computational complexity of the algorithms and introduced additional parameters. The first step to reducing the need for such involved local processing was to avoid the over-exposure of bright regions while enhancing the dark regions. Initial logarithmic solutions were not effective and flattened the images in addition to fading colours; thus, a new formulation for the global contrast operator had to be devised to achieve this objective.

3.1.1 Gain offset correction-based stretching (GOCS)

The expression for the GOC algorithm [57] is given as shown in (1);

$$I_{o_{GOC_2}} = \left[\frac{L-1}{I_{max}-I_{min}}\right](I_i - I_{min}), \quad (1)$$

The contrast stretching algorithm is given as;

$$I_{o_{CS}} = \left[\frac{I_{max}-I_{min}}{I_{high}-I_{low}}\right](I_i - I_{low}) + I_{min}, \quad (2)$$

In (4) and (5), $I_{o_{GOC_2}}$ and $I_{o_{CS}}$ are the enhanced images using GOC and CS respectively, I_{max}, I_{min} are maximum and minimum pixel intensities in the input image, I_i, L is the number of grey intensity levels (L =256 for unsigned integer, eight-bit-per-pixel (uint8, 8bpp) image format), while I_{low} and I_{high} are the lower and upper percentiles of the image pixel intensity distribution normally set at 5% and 95% respectively.

The faults of the GOC lie in the statistics such as maximum and minimum pixel intensity values utilized in its computation. Since an image which is already utilizing its full dynamic range will not be affected by such statistics, we needed to realize a more influential statistic. The contrast stretching operator utilizes lower and upper percentiles of the image intensity distribution for its computation and as a result, does not suffer over-exposure effects and performs adequate contrast enhancement. Conversely, the GOC performs sufficient colour correction but minimal contrast enhancement. Thus, by replacing the maximum and minimum pixel intensity values with the upper and lower percentiles in the formulation, we can realize a new formula for the global contrast operation as;

Preprints (www.preprints.org) | NOT PEER-REVIEWED | Posted: 22 July 2018 doi:10.20944/preprints201807.0402.v1

Peer-reviewed version available at J. Imaging 2018, 4, 108; doi:10.3390/jimaging4090108

$$I_{o_{GOCS}} = \left[\frac{L-1}{I_{high}-I_{low}}\right](I_i - I_{low}), \quad (3)$$

Initial experiments using the 5th and 95th percentiles led to some pixels being over-exposed and as we widened the range between the percentiles, the results improved and in some cases, settled on the 1st and 99th percentiles for best results. Increasing the range to its maximum yields a result similar to GOC as expected since the high and low percentiles now become the maximum and minimum pixel intensity values. The GOCS is related to the CS in the following form;

$$I_{o_{CS}} = I_{o_{GOCS}}(I_{max} - I_{min}) + I_{min}, \quad (4)$$

3.2 Proposed multi-scale local contrast operator

We present the development of the multi-scale algorithm for local contrast enhancement, which replaces the CLAHE used in previous work, drastically reducing complexity and run-time.

3.2.1 Modified spatial filter-based enhancement

Given a filter-based approach to contrast enhancement and illumination correction [53];

$$I_o(x,y) = I_{HPF}(x,y) + [I_{LPF}(x,y)]^k, \quad (5)$$

Where the high-pass filtering operation was expressed as;

$$I_{HPF}(x,y) = -\nabla I(x,y) \; or \; -\nabla^2 I(x,y) \quad (6)$$

And the low-pass filtering was expressed as;

$$I_{LPF}(x,y) = I(x,y) + \nabla I(x,y) \; or \; I(x,y) + \nabla^2 I(x,y) \quad (7)$$

And using the isotropic heat diffusion equation;

$$\frac{\partial I(x,y)}{\partial t} = -\nabla^2 I(x,y) \quad (8)$$

The high-pass and low-pass filtering operations is redefined as;

$$I^{t+1}(x,y) = I^t(x,y) - \nabla^2 I(x,y)\Delta t \quad (9)$$

and

$$I^{t+1}(x,y) = I^t(x,y) + \nabla^2 I(x,y)\Delta t \quad (10)$$

This was further expanded into PDE-based formulations [53] as;

$$I_o(x,y) = -\nabla I(x,y) + [D-1]^{1-k}\{I(x,y) + \nabla I(x,y)\}^k \quad (11)$$

$$I_o(x,y) = -\nabla^2 I(x,y) + [D-1]^{1-k}\{I(x,y) + \nabla^2 I(x,y)\}^k \quad (12)$$

Subsequently, fractional derivative-based re-definitions for high- and low-pass filtering of arbitrary order α are obtained as;

$$I_{HPF}(x,y) = -\nabla^\alpha I(x,y) \quad (13)$$

and

$$I_{LPF}(x,y) = \int_\Omega I_{HPF}(x,y)d\Omega = -\int_\Omega \nabla^\alpha I(x,y)d\Omega = I(x,y) + \nabla^\alpha I(x,y) \quad (14)$$

Leading to the expression;

$$I_e(x,y) = -\nabla^\alpha I(x,y) + [I(x,y) + \nabla^\alpha I(x,y)]^k \quad (15)$$

We further extend the application to hazy image enhancement as;

$$U(x,y) = I_{max} - I(x,y) \quad (16)$$

$$U_e^\alpha(x,y) = -\nabla^\alpha U(x,y) + \left[-\int_\Omega \nabla^\alpha U(x,y)d\Omega\right]^k \quad (17)$$

$$I_e^\alpha(x,y) = U_{e_{max}}^\alpha - U_e^\alpha(x,y) \quad (18)$$

Preprints (www.preprints.org) | NOT PEER-REVIEWED | Posted: 22 July 2018 doi:10.20944/preprints201807.0402.v1

Peer-reviewed version available at J. Imaging 2018, 4, 108; doi:10.3390/jimaging4090108

In the latter expressions of eqn. (16) to (18), $U(x,y)$ is the inverted image, I_{max} is the maximum pixel intensity of the input image, $I(x,y)$, $\nabla^{\alpha}U(x,y)$ is the fractional derivative of the inverted image and $\int_{\Omega}\nabla^{\alpha}U(x,y)d\Omega$ denotes the fractional order integral. Additionally, $U_e^{\alpha}(x,y)$ is the enhanced inverted image using fractional order-based operations and $U_{e_{max}}^{\alpha}$ is the maximum pixel intensity of $U_e^{\alpha}(x,y)$ while $I_e^{\alpha}(x,y)$ is the de-hazed image using fractional order-based operations. Additionally, we wish to reduce the computational load of computing both the derivative and the integral, especially in the fractional order-based version. Thus, we simple obtain the fractional integral of the input image and subtract it from the original image and multiply by the appropriate factor to obtain the fractional order derivative. This saves resources especially on digital hardware implementations since only one operator is utilized and re-used. This is easily expressed as;

$$I_{HPF}(x,y) = I(x,y) - I_{LPF}(x,y) \tag{19}$$

$$I_o(x,y) = \gamma[I(x,y) - I_{LPF}(x,y)] + [I_{LPF}(x,y,t)]^k \tag{20}$$

Which gives the expressions in both integer and fractional order calculus as;

$$I_o(x,y) = \gamma\left[I(x,y) - \left\{\int_{\Omega}\nabla I(x,y)d\Omega\right\}\right] + \left[\int_{\Omega}\nabla I(x,y)d\Omega\right]^k \tag{21}$$

$$I_o(x,y) = \gamma\left[I(x,y) - \left\{\int_{\Omega}\nabla^{\alpha} I(x,y)d\Omega\right\}\right] + \left[\int_{\Omega}\nabla^{\alpha} I(x,y)d\Omega\right]^k \tag{22}$$

The scheme for hazy image enhancement can also be updated accordingly without much effort.

3.2.2 Multi-scale illumination/reflectance contrast enhancement (Multi-IRCES)

The central idea is that by further decomposing a low-pass filtered image and enhancing the details at each level and recombining the results, we would obtain much finer local enhancement. Additionally, using the fractional order reduces or minimizes the issue of noise enhancement as high frequency components are amplified at each stage, further reducing or minimizing the low frequency components at each stage. Since the haze is a low frequency phenomenon, we expect that such effects would be greatly reduced after processing without enhancing noise. The entropy and standard deviation measures are utilized to select the best outcome for the processed image in terms of the value of the exponent, k. The mathematical expressions for the algorithm are as shown in (23) to (29);

$$I_i(x,y) = I_{HPF_i}(x,y) + \left[I_{LPF_i}(x,y)\right]^k ; i = 0,1,\dots,N-1 \tag{23}$$

$$I_{A_k}(x,y) = \frac{1}{N}\sum_{i=0}^{N-1} I_i(x,y); k = 2 \tag{24}$$

$$I_{B_k}(x,y) = \frac{1}{N}\sum_{i=0}^{N-1} I_i(x,y);\ \ k = 0.5 \tag{25}$$

$$e_{A_k} = entropy(I_{A_k}); e_{B_k} = entropy(I_{B_k}) \tag{26}$$

$$\sigma_{A_k} = std(I_{A_k}); \sigma_{B_k} = std(I_{B_k}) \tag{27}$$

$$f(x,y) = \begin{cases} I_{A_k}(x,y), & e_{A_k} > e_{B_k}\ or\ \sigma_{A_k} > \sigma_{B_k} \\ I_{B_k}(x,y), & e_{A_k} < e_{B_k}\ or\ \sigma_{A_k} < \sigma_{B_k} \end{cases} \tag{28}$$

$$f_o(x,y) = GOCS[f(x,y)] \tag{29}$$

In eqn. (23), $I_i(x,y)$ is the enhanced image at level i and N is the number of decomposition levels, while $I_{HPF_i}(x,y)$ and $I_{LPF_i}(x,y)$ are high-pass and low-pass filtered images obtained at level i. Based on experiments, we set $N = 5$. The obtained level images are then aggregated to obtain the

Preprints (www.preprints.org) | NOT PEER-REVIEWED | Posted: 22 July 2018 doi:10.20944/preprints201807.0402.v1

Peer-reviewed version available at J. Imaging 2018, 4, 108; doi:10.3390/jimaging4090108

final images, I_{A_k} or I_{B_k} for the different values of the power factor, k in (24) and (25). The values for the power factor are chosen to be multiples of two (2) due to hardware design considerations to enable fast computation by bit shifting.

The respective entropies (e_{A_k}, e_{B_k}) and standard deviations (σ_{A_k}, σ_{B_k}) of the aggregated images are computed (in eqns. (26) and (27)) and used to decide the best image outcome, $f(x,y)$ in (28), which is then processed with the modified global contrast enhancement algorithm to obtain the final output image, $f_o(x,y)$ in (29). This is based on the simultaneous multi-level high frequency component (edges and details) enhancement and multi-level low frequency component attenuation.

All processing operations are achieved with spatial filter kernels using fractional order-based calculus, which slightly increases computation cost but also yields better results in terms of balanced edge enhancement. However, we can also save on computation by utilizing integer-order-based calculus for the kernel coefficients, though results will be more drastic. The diagram of the proposed algorithm for enhancement of both hazy and underwater images is shown in Fig. 1. All processing operations are achieved with spatial filter kernels using fractional order-based calculus, which slightly increases computation cost but also yields better results in terms of balanced edge enhancement. However, we can also save on computation by utilizing integer-order-based calculus for the kernel coefficients, though results will be more drastic.

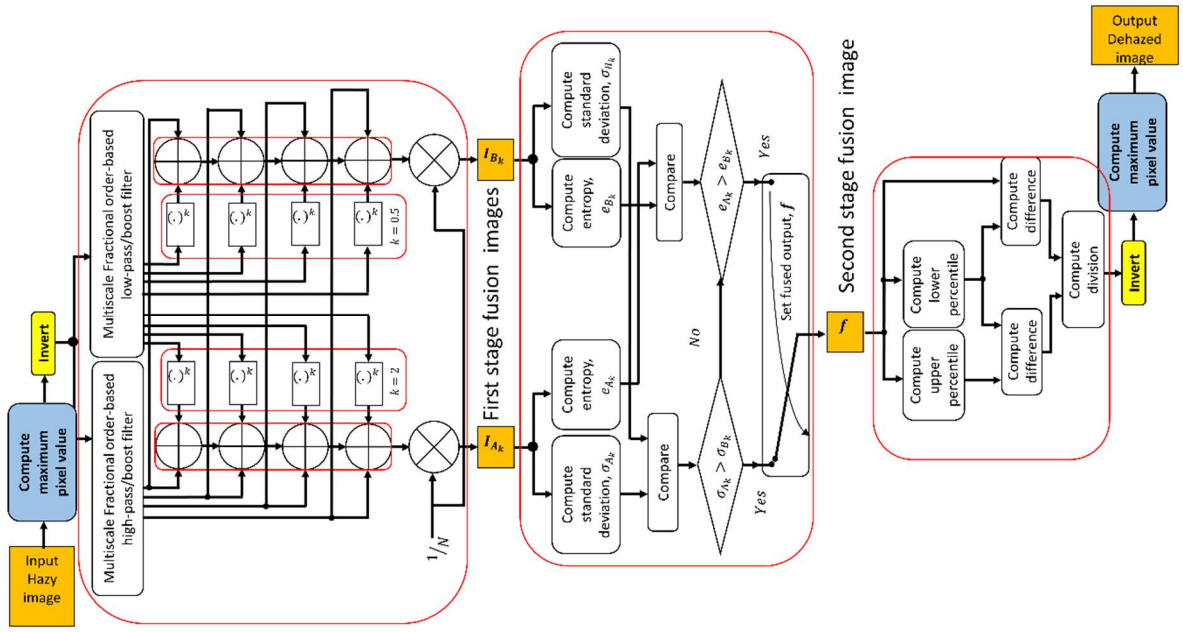

Figure 1. Proposed algorithm (PA) for enhancing hazy and underwater images

3.2.3 Preliminary results

After testing several images, it was discovered that some images were better enhanced when using the 5th and 95th percentiles rather than the 1st and 99th percentiles. The representative images of these two groups include those unaffected by wide ranges while the other exhibits over-exposure for narrow ranges. This was partly the reason that the PWL approach was utilized in previous work [27]. Thus, one approach would be to devise a means of selecting the appropriate percentiles for these two groups of images. A simple compromise was to set the range between the 2nd and 98th percentiles. However, we would still be faced with the issue of outlier images, which resist colour correction attempts. Thus, the need for the localized operator to aid in the detail recovery in the otherwise over-

Peer-reviewed version available at J. Imaging 2018, 4, 108; doi:10.3390/jimaging4090108

exposed regions when global contrast operations are performed. In Fig. 2, a sample result of the algorithm is shown for high-pass and high-boost configurations. The latter is used to minimize edge and noise over-enhancement, while the former improves details in the processed images as shown.

(a) **(b)** **(c)**

Figure 2. (a) Underwater image enhanced with (b) PA using high-pass and (c) high-boost fractional filter settings

3.3 Problems and solutions

The initial developed scheme worked extremely well for underwater images and several hazy images. However, problems were observed in other hazy images. These issues included colour fading, distortion, discolouration, image darkening, inadequate haze removal, and over-enhanced edges. Thus, we devised solutions to some of these problems. The colour correction routine was omitted and the output, $f(x,y)$ was reformulated as;

$$f(x,y) = \frac{I_{A_k}(x,y) + I_{B_k}(x,y)}{2} \tag{30}$$

This improved results and resolved colour distortion in the affected hazy images, though there was some colour fading in RGB and HSI/HSV versions. Thus, we utilized the red-green-blue-intensity/value (RGB-IV) formulation [58] to improve colour rendition, which resulted in colour enhancement but with dark images. We also investigated the use of CLAHE to improve local contrast, resulting in drastic improvements. However, enhanced images also exhibited halo effects and colour distortion, which persisted despite combination with the multi-scale IRCES algorithm. Furthermore, there was drastic colour loss/fading using CLAHE in addition to increased computational complexity, defeating the initial objective of the proposed approach. Thus, alternatives were considered to resolve these issues.

Wavelet-based fusion of $I_{A_k}(x,y)$ and $I_{B_k}(x,y)$ using mean, minimum or maximum configurations was implemented. Good results were observed in images with mostly uniform haze. Conversely, sky regions were degraded in hazy images with uneven haze or considerable sky regions. Furthermore, dark bands and outlines were observed around edges in some processed images. Overall, image results were inconsistent using this scheme. Thus we reformulated the multi-scale algorithm after extensive analysis.

Redundant frequencies, which were unnecessary in hazy image enhancement results were observed. This was due to the nature of the generation of the two combined images; $I_{A_k}(x,y)$ and $I_{B_k}(x,y)$, leading to unbalanced contributions of frequency components. Constant varying of weights for both images and corresponding results led to inconsistent results. Thus, a more formalized, systematic approach was required. Based on analysis of the Fourier Transform of the images, we

Peer-reviewed version available at J. Imaging 2018, 4, 108; doi:10.3390/jimaging4090108

require subtle enhancement of the high frequency components and a drastic reduction of the contributions of the low frequency components. This informed the reformulation of the multi-scale algorithm for hazy images as;

$$I(x,y) = U_{max} - U(x,y) \tag{31}$$

$$\{I_{LPF_i}(x,y), I_{HPF_i}(x,y)\} = decompose(I(x,y)) \tag{32}$$

$$S_{LPF_i} = \sum_{x=0}^{N-1}\sum_{y=0}^{M-1} I_{LPF_i}(x,y) \tag{33}$$

$$S_{HPF_i} = \sum_{x=0}^{N-1}\sum_{y=0}^{M-1} I_{HPF_i}(x,y) \tag{34}$$

$$S_{total} = S_{LPF_i} + S_{HPF_i} \tag{35}$$

$$p_{LPF_i} = \frac{S_{LPF_i}}{S_{total}};\ p_{HPF_i} = \frac{S_{HPF_i}}{S_{total}} \tag{36}$$

In the expressions, (31) to (36), $U(x,y)$ and $I(x,y)$ are the original and reversed hazy image, respectively, while U_{max} is the maximum pixel intensity value of the image; $I_{LPF_i}(x,y)$, $I_{HPF_i}(x,y)$, S_{LPF_i} and S_{HPF_i} are the low- and high-pass filtered images of level (or scale), i and their respective summations. The terms S_{total}, p_{LPF_i}, p_{HPF_i} are the total sum, and percentage of low and high frequency components, respectively. In order to balance the high and low frequency components, we create new constants, c_1 and c_2 to be dependent on each other using the percentages;

$$c_1 = \frac{1}{p_{LPF_i}};\ c_2 = \frac{1}{c_1} \tag{37}$$

After evaluation of the two constants, we use the expression to obtain the enhanced level image as;

$$I_i(x,y) = c_1\left[I_{HPF_i}(x,y)\right] + \left[I_{LPF_i}(x,y)\right]^{c_2} \tag{38}$$

The level images are subsequently summed to obtain the enhanced image as shown in (39);

$$f(x,y) = \frac{1}{D-1}\sum_{i=0}^{D-1} I_i(x,y) \tag{39}$$

The de-hazed image, $U'(x,y)$ is obtained by inverting the image as shown;

$$U'(x,y) = f_{max} - f(x,y) \tag{40}$$

Based on experiments, we set c_1 and c_2 as 1.21 and 0.8264 respectively since they are always constant. These are the default values for balanced enhancement of high and low frequency components to avoid visual artefacts. However, the values may be increased or decreased gradually for maximum visual effect in certain images. This new formulation solves the edge over-enhancement, colour distortion and halo effect problem. The results are shown in Fig. 3 for processed images using previous and improved configurations of PA. Note the elimination of the colour distortion and reduced degree of noise enhancement for images in Fig. 3(b) compared to Fig. 3(a).

The estimated computational complexity of the proposed approach is given as; $O(NMw^2D)$ for D levels using spatial window size, w of fractional order-based filter for an image with N rows and M columns. Additionally, the algorithm can be speeded up by exploiting symmetric convolutional structures to reduce the number of multiplications and additions.

Peer-reviewed version available at J. Imaging 2018, 4, 108; doi:10.3390/jimaging4090108

(a)

(b)

Figure 3. Processed images using (a) previous configuration (b) improved configuration of PA

4. Results

We present the result comparisons of the proposed approach (PA) with other algorithms from the literature. We utilize metrics such as entropy (E), (relative) average gradient (RAG) [59], global contrast factor (GCF) [60], colourfulness or colour enhancement factor (CEF) [61] for underwater images. For hazy images, we utilize the RAG, ratio of visible edges, Q_e [1] and saturation parameter/percentage of black or white pixels, σ [1] to evaluate results. Higher values indicate better results for the first two metrics while lower values imply improvement for the last metric. The hardware specifications of the computing platform are: PC with Intel® Core i7-6500U x64-based processor at 2.5GHz/2.59GHz, 12 GB RAM running 64-bit OS (Microsoft® Windows™ 10 Home) and NVIDIA® GeForce™ 940M GPU with compute capability of 5.0.

4.1 Underwater images

Results are presented in Fig. 4, which contains results from [5], amended with results from [27] and PA and show that there is a considerable contrast and edge enhancement as details are seen much more clearly with minimal haze. For the *fish* image in Fig. 4, only results by Ancuti, et al [62], Fu et al [15], Galdran, et al [4], PDE-based PWL-CLAHE (forward and reverse configuration) [27] and PA yield good results. The rest of the image results depict hazy, faded images with large degree of green colouration, while Li, et al's method [5] yields an image with reddish colouration, implying over-compensation of red channel in the processed image.

Peer-reviewed version available at J. Imaging 2018, 4, 108; doi:10.3390/jimaging4090108

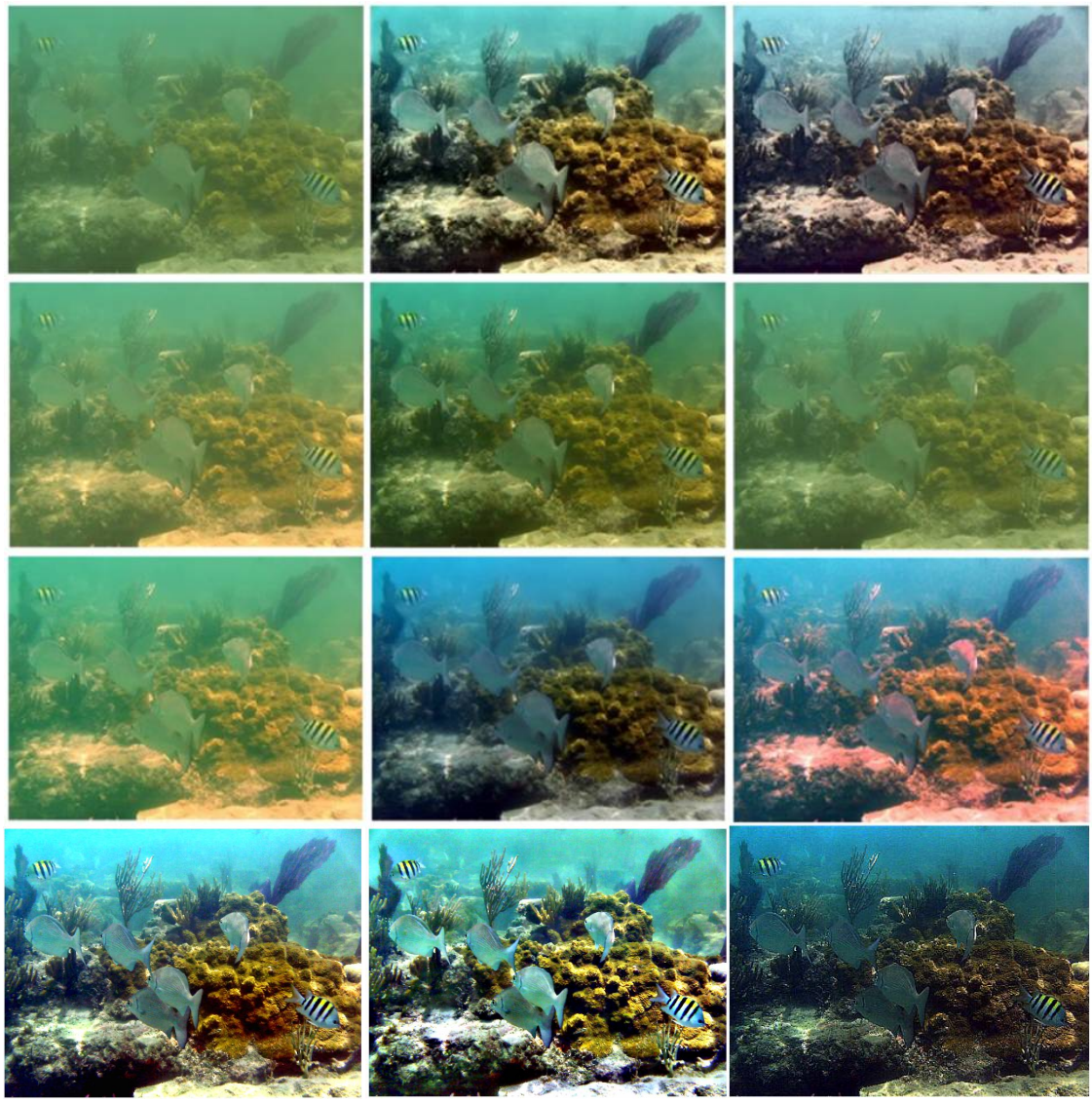

KEY

(a)	*(b)*	*(c)*
(d)	*(e)*	*(f)*
(g)	*(h)*	*(i)*
(j)	*(k)*	*(l)*

Figure 4. (a) Original *Fish2* image processed with algorithms proposed by (b) Ancuti *et al* [62] (c) Fu *et al* [15] (d) Chiang and Chen [8] (e) He *et al* [32] (f) Carlevaris-Bianco *et al* [11] (g) Serikawa and Lu [10] (h) Galdran *et al* [4] and (i) Li *et al* [5], and IPA using (j) PWL-CLAHE and (k) CLAHE-PWL-AD configurations (l) PA

Based on the results, the proposed algorithm yields finer and sharper edges and details with minimal intrinsic noise due to the fractional derivative ability. The visual results are mostly reflected in the quantitative metrics shown in Table 1, with PA showing the highest AG values, indicating more visible edges and details especially on the rock face of the bottom left corner of the image

(image(l)). However, PDE-GOC2-CLAHE yields the highest colourfulness (C) and entropy while the method by Fu, et al gives best GCF value (though there is over-exposure in the bright regions of the rock faces in image (c)).

Table 1. Comparison of IPA with various algorithms for *Fish2* image

Measures \Algos	Ancuti [62]	Bianco [11]	Chiang [8]	Fu [15]	Galdran [4]	He [32]	Li [5]	Serikawa [10]	(PDE-PWL-CLAHE) [27]	PA
Entropy	7.8438	7.1251	7.2986	7.8628	7.6376	7.4587	7.7168	7.4531	**7.8945**	7.2558
GCF	9.5759	4.6944	3.9611	**9.6404**	8.7299	6.372	7.0632	4.9016	8.6257	6.9014
C	54.5704	42.3128	54.8975	36.337	64.0309	57.0533	63.8498	63.2207	**77.5420**	61.1957
AG	9.1638	4.1501	4.1285	9.4732	5.6937	5.174	7.6573	5.2034	10.4343	**13.9107**

4.2 Hazy image enhancement results

We also present results and comparisons for hazy image contrast enhancement with algorithms from the literature using 53 real benchmark images employed in de-hazing experiments. Also, the FRIDA3 dataset [63] [64] consisting of left and right views of 66 synthetic images was also tested. The algorithms include Tarel and Hautiere [65], Dai et al [66], Nishino et al [67], He et al [32], Galdran et al [41], Wang and He [68], Zhu et al [69], Ren et al [46], partial differential equation-based single scale Retinex GOC-CLAHE (PDE-GOC-SSR-CLAHE) [52], PDE-IRCES [53], and PA. The proposed approach (PA) is much more vivid as it enhances edges and avoids discolouration of sky regions as seen in the *Tiananmen* image in Fig. 5. Best results are observed for PA, Ren, et al [46], Zhu, et al [69] and He et al [32] (has halos) followed by PDE-GOC-SSR-CLAHE [52] (has some halos) and PDE-IRCES [53] (no halos but under-enhanced in some regions).

The method by Tarel and Hautiere [65] shows over-enhancement of edges and discolouration of sky region similarly to PDE-IRCES. The method by Ren, et al shows sharpened features without sky discolouration or over-enhancement similar to Zhu, et al (which is darker). The PDE-GOC-SSR-CLAHE yields considerable detail in non-homogeneous regions, while PA yields the highest detail and edge enhancement without sky discolouration or halo effects. The same is observed for the *toys* image in Fig. 6 as the image obtained from PA has the most enhanced edges and details compared to the other results. The PDE-GOC-SSR-CLAHE gives best local contrast enhancement, followed by the DCP method by He et al, and the methods by Wang, et al [68], Ren et al, Dai, et al [66] and Zhu, et al. The rest of the other image results are faded and still contain a reasonable amount of haze or have colour distortion or saturation with minimal edge enhancement.

Peer-reviewed version available at J. Imaging 2018, 4, 108; doi:10.3390/jimaging4090108

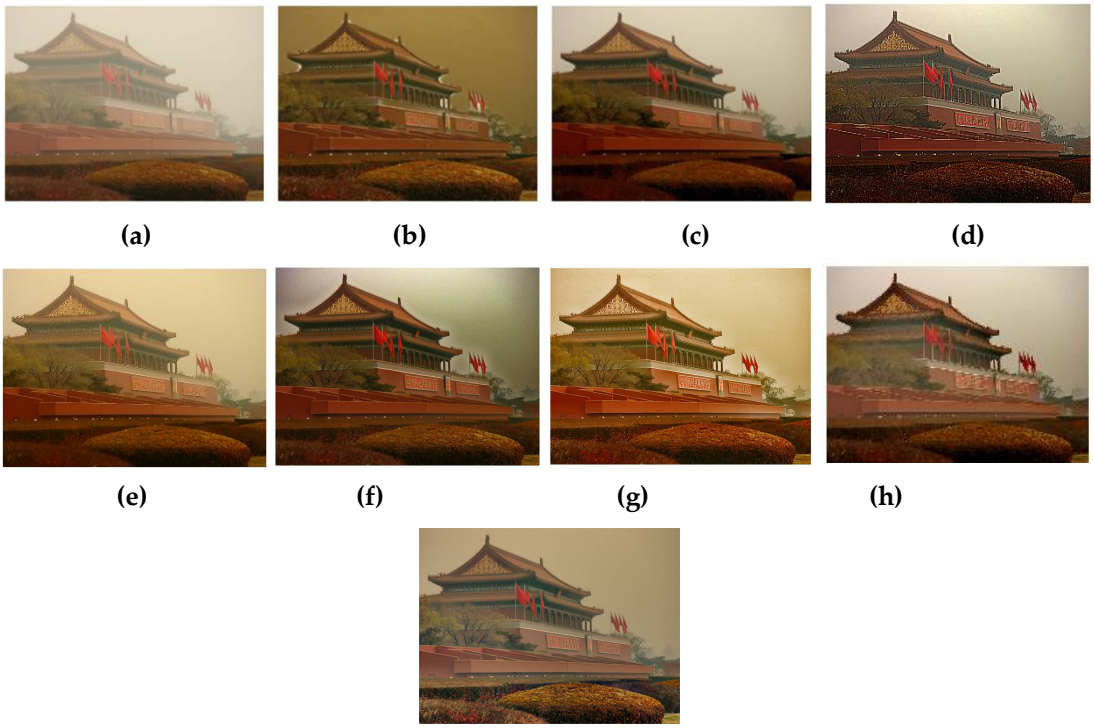

Figure 5. (a) Original hazy image (b) Tarel, et al (c) Zhu, et al (d) PA (e) PDE-IRCES (f) He, et al (g) PDE-GOC-SSR-CLAHE (h) Ren et al (i) AMEF

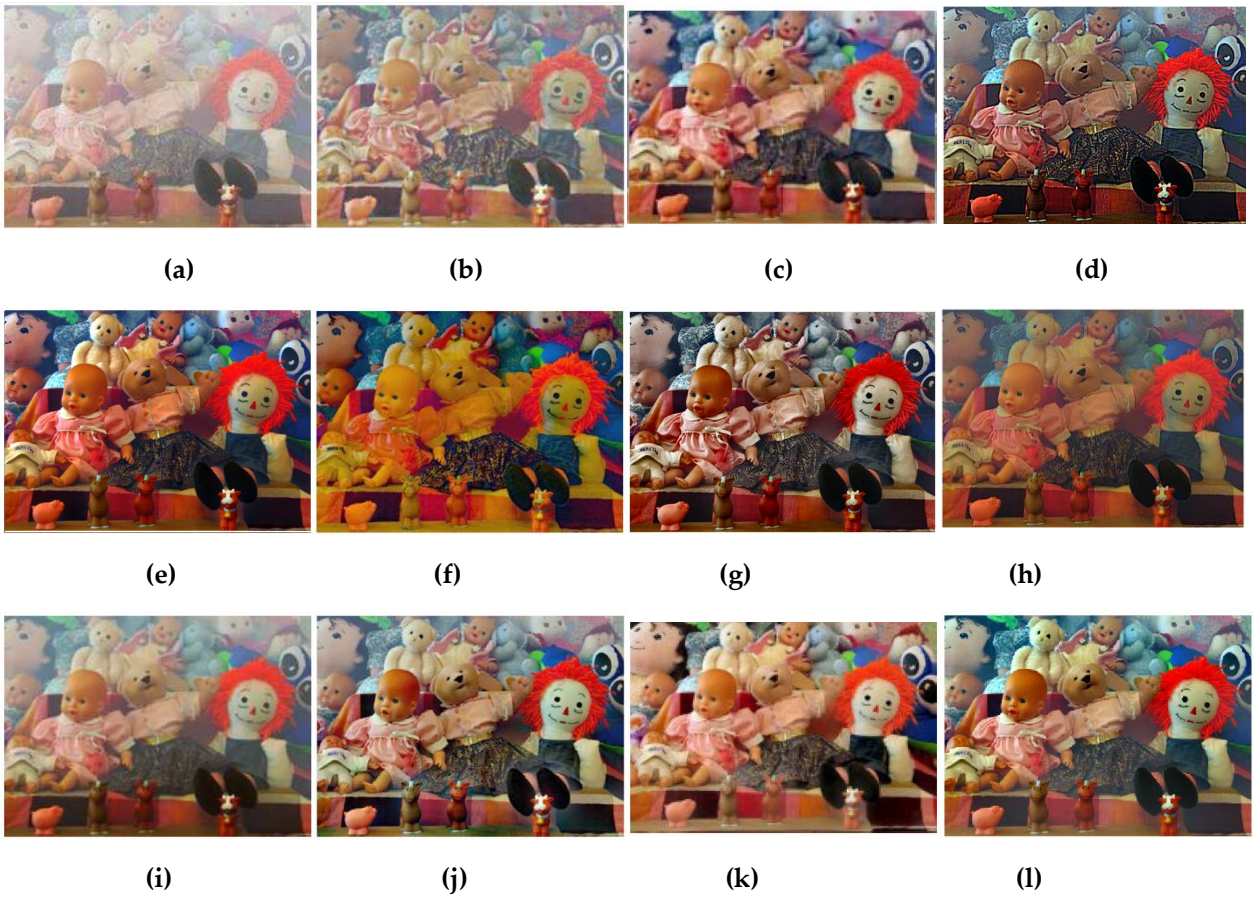

Peer-reviewed version available at J. Imaging 2018, 4, 108; doi:10.3390/jimaging4090108

(m)

Figure 6. (a) Original hazy image (b) Tarel, et al [65] (c) Dai et al [66] (d) PA (e) He et al [32] (f) Nishino, et al [67] (g) PDE-GOC-SSR-CLAHE [52] (h) PDE-IRCES [53] (i) Galdran, et al (EVID) [41] (j) Wang & He [68] (k) Zhu, et al [69] (l) Ren, et al [46] (m) AMEF

Additionally, we present the numerical results for the available algorithm implementations compared with PA in Table 2. Results indicate that RAG and ratio of visible edge values are the highest for PA, followed by PDE-GOC-SSR-CLAHE, He et al and Ren, et al. Thus, these two metrics indicate maximum edge enhancement corresponding to increased visibility and haze removal. The value of the Canon image yields the highest RAG value and the image result (not shown) depicted drastic edge and detail enhancement.

The PA can also be configured to process only the intensity channel for hazy images using the HSI and HSV colour spaces to avoid hue distortion. However, the algorithm was initially conceived in the RGB space to enable the processing of both underwater and hazy colour images without need for modification. We also present the runtimes of PA in comparison with the other approaches in Table 3 and Fig. 7 to further showcase the low computational complexity of the algorithm. Only the method by Ren et al is fully optimized for GPU computation, with PA and other algorithms using parallel computation where possible. Results indicate that PA is the fastest algorithm of all the compared ones. Furthermore, the revised formulation combined with the RGB-IV does not increase run-time considerably, except for images with very large dimensions. Nevertheless, the run-time is still much less than the algorithms by He et al, Zhu et al and Ren et al. The revised scheme is also much easier to implement in FPGA hardware than the earlier version due to absence of global statistical computation.

Additionally, we present the relative average gradient (RAG) values for the available algorithm implementations compared with the proposed approach in Table 2. Results indicate improvements using the proposed approach and the RAG values are the highest for the PA, followed by PDE-GOC-SSR-CLAHE, He et al and Ren, et al. Thus, such RAG values indicate maximum edge enhancement corresponding to increased visibility and haze removal. The value of the Canon image yields the highest RAG value and the image result (not shown) depicted drastic edge and detail enhancement.

Peer-reviewed version available at J. Imaging 2018, 4, 108; doi:10.3390/jimaging4090108

468 **Table 2**. RAG, ratio of visible edges and saturation parameter values for images processed with He
469 et al [32], Zhu, et al [69], Ren, et al, PDE-GOC-SSR-CLAHE [52], PDE-IRCES [53] and PA

Algos / **Images**	**He, et al** [32] (Ω = 0.95, w = 15, A = 240, r = 24)	**Zhu, et al** [69] β=0.95,1; θ_0=0.1893; θ_1=1.0267; θ_2=−1.2966; Guided filter: r=60; t_0=0.05; t_1=1; ε=0.001	**Ren et al** [46] γ=1.3 (*canyon* image) 0.8≤γ≤1.5 (others)	**PDE-GOC-SSR-CLAHE** [52] Δt=0.25; k_{sat}=1.5	**PDE-IRCES** [53] Δt=0.25	**PA**
Tiananmen	1.8455 /0.9606 /0.1879	1.1866 /1.0041 /0.0814	1.5649 /0.8734 /0.1288	2.8225 /1.0386 /0.0625	2.3219 /1.1614 **/0**	**4.4410 /1.4514** /0.1688
Cones	1.4977 /1.1478 /0.3878	0.9704 /1.0873 /0.2499	1.3818 /1.1042 /0.2956	2.7516 **/1.1999** /0.2733	2.5881 /1.2064 **/0**	**4.9702 /1.4620** /0.3142
City1	1.1914 /1.0332 /0.1336	0.9303 /1.0075 /0.2002	1.2989 /1.0232 /0.2002	1.7762 /1.1164 /0.0562	2.4080 /1.3458 **/0.00375**	**3.8282 /1.4898** /0.1712
Canyon	1.7481 /1.1057 /0.3796	1.2880 /1.0679 /0.2412	1.4564 /1.0319 /0.0446	2.5408 /1.2070 /0.3103	2.5224 /1.19684 **/0.00019**	**3.9892 /1.7903** /0.2412
Canon	3.2903 /1.0857 /0.3947	1.7127 /0.9089 /0.3198	2.6871 /1.0832 /0.3831	2.8059 /1.1188 /0.3947	2.8783 **/1.3450** **/4.4E-05**	**8.0224 /1.5785** /0.3942
Mountain	1.7105 /0.9348 /0.0787	1.2092 /0.9307 /0.0984	1.6005 /0.9784 /0.0074	2.7275 /1.0202 /0.0074	2.9827 /1.2977 **/7.1E-05**	**6.5399 /1.5503** /0.0244
Brickhouse	1.2006 /0.9747 /0.1172	0.8597 /1.1395 /0.0730	1.2118 /1.0030 /0.1288	1.0836 /1.1135 /0.1021	1.4105 /1.2789 **/0**	**3.0014 /1.3563** /0.0983
Pumpkins	1.5927 /0.9501 /0.1581	0.9311 /0.6726 /0.1333	1.4753 /0.9511 /0.1764	2.4539 /1.0361 /0.1516	2.2777 /1.1626 **/7.1E-05**	**3.3553 /1.6469** /0.2329
Train	1.5206 /1.0090 /0.1664	0.9797 /1.0509 /0.3265	1.2036 /1.0203 /0.2412	1.5190 /1.1106 /0.3005	2.2569 /1.3589 **/0.0038**	**4.3014 /1.5151** /0.2594
Toys	2.2566 /0.9712 /0.3840	1.6711 /1.0117 /0.2865	2.1568 /0.9576 /0.2827	2.9813 /1.1095 /0.3379	2.1367 /1.2887 **/2.8E-05**	**4.2837 /1.5937** /0.3736

470
471

Preprints (www.preprints.org) | NOT PEER-REVIEWED | Posted: 22 July 2018 doi:10.20944/preprints201807.0402.v1

Peer-reviewed version available at J. Imaging 2018, 4, 108; doi:10.3390/jimaging4090108

Table 3. Runtimes for hazy images processed with He et al [32], Zhu, et al [69], Ren, et al, AMEF, PDE-GOC-SSR-CLAHE [52], PDE-IRCES [53] and PA

Algos / Images	He, et al [32]	Zhu, et al [69]	Ren et al [46]	AMEF [54]		PDE-GOC-SSR-CLAHE [52]	PDE-IRCES [53]	PA
Tiananmen(450×600)	1.253494	0.991586	2.362754	1.4088		3.530989	2.330879	**0.480659**
Cones (384×465)	0.850155	0.661314	1.651447	1.0506		2.381621	1.555098	**0.268909**
City1(600×400)	1.094910	0.875287	2.070620	1.2709		3.203117	2.183417	**0.283372**
Canyon (600×450)	1.237655	0.972741	2.529734	1.5066		3.821395	2.306129	**0.309343**
Canon (525×600)	1.431257	1.135376	2.890541	1.6958		4.187972	2.717652	**0.374638**
Mountain (400×600)	1.129231	0.880835	2.358143	1.2985		3.158335	2.055685	**0.360240**
Brickhouse(711×693)	2.230871	1.667610	5.234674	2.3618		6.395965	4.385789	**1.102332**
Pumpkins (400×600)	1.125475	0.901815	2.253179	1.5018		3.152969	2.143529	**0.407310**
Train (400×600)	1.105757	0.849072	2.075004	1.2935		3.178277	1.995436	**0.365481**
Toys (360×500)	0.844945	0.657376	1.578068	1.0387		2.429651	1.545031	**0.260878**

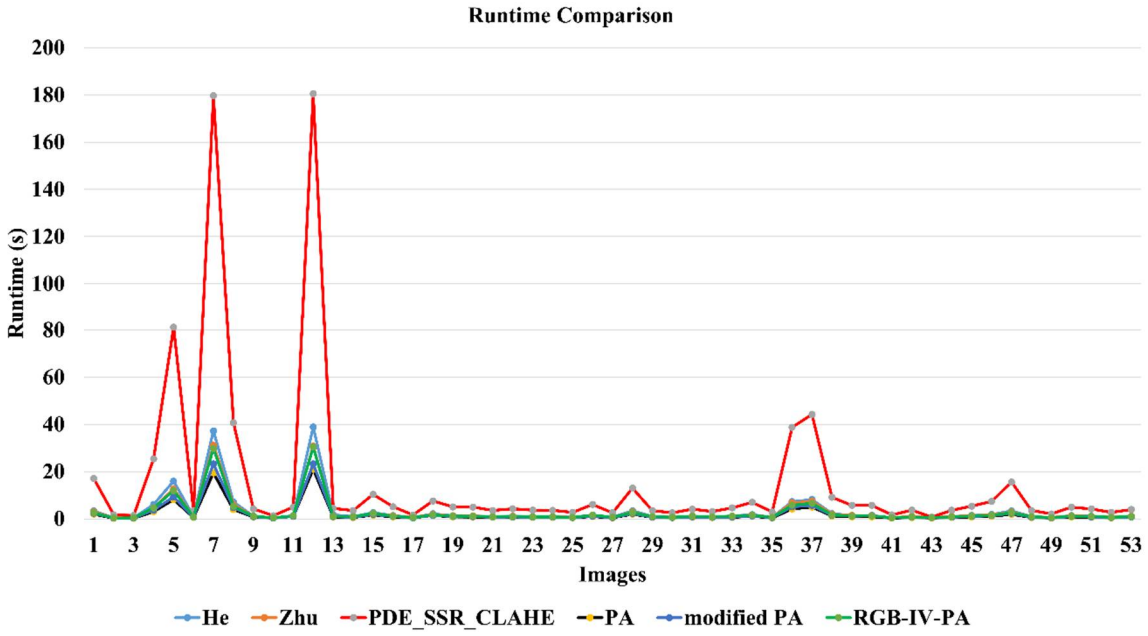

(a)

Preprints (www.preprints.org) | NOT PEER-REVIEWED | Posted: 22 July 2018 doi:10.20944/preprints201807.0402.v1

Peer-reviewed version available at J. Imaging 2018, 4, 108; doi:10.3390/jimaging4090108

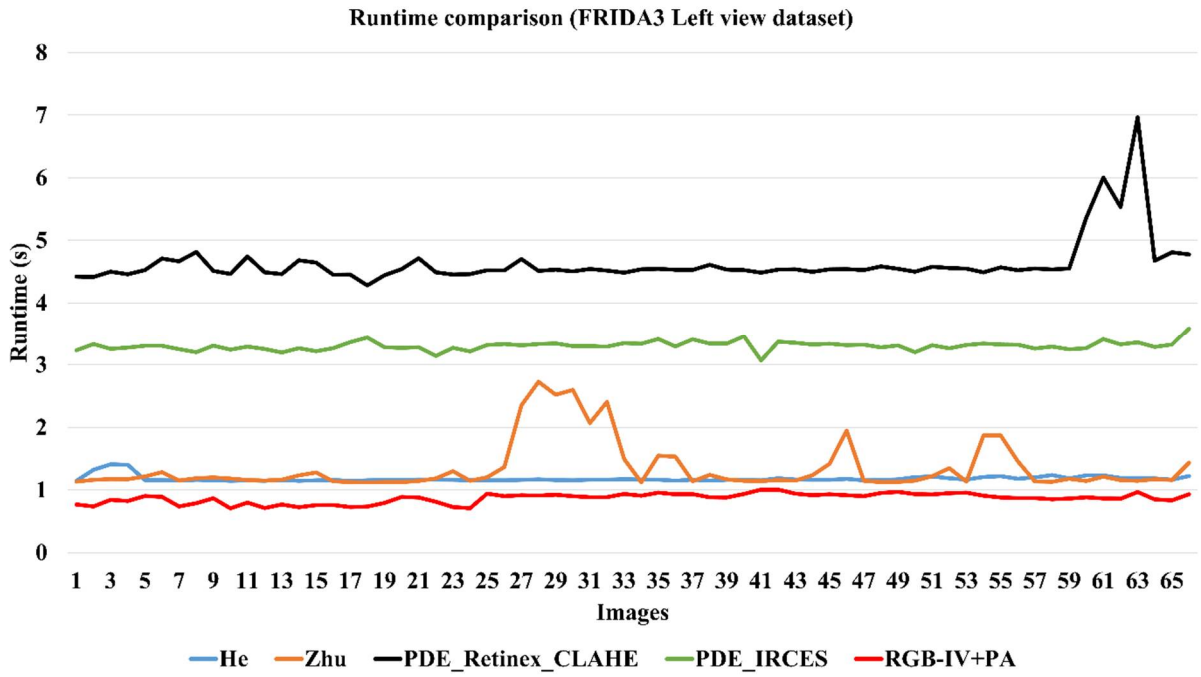

(b)

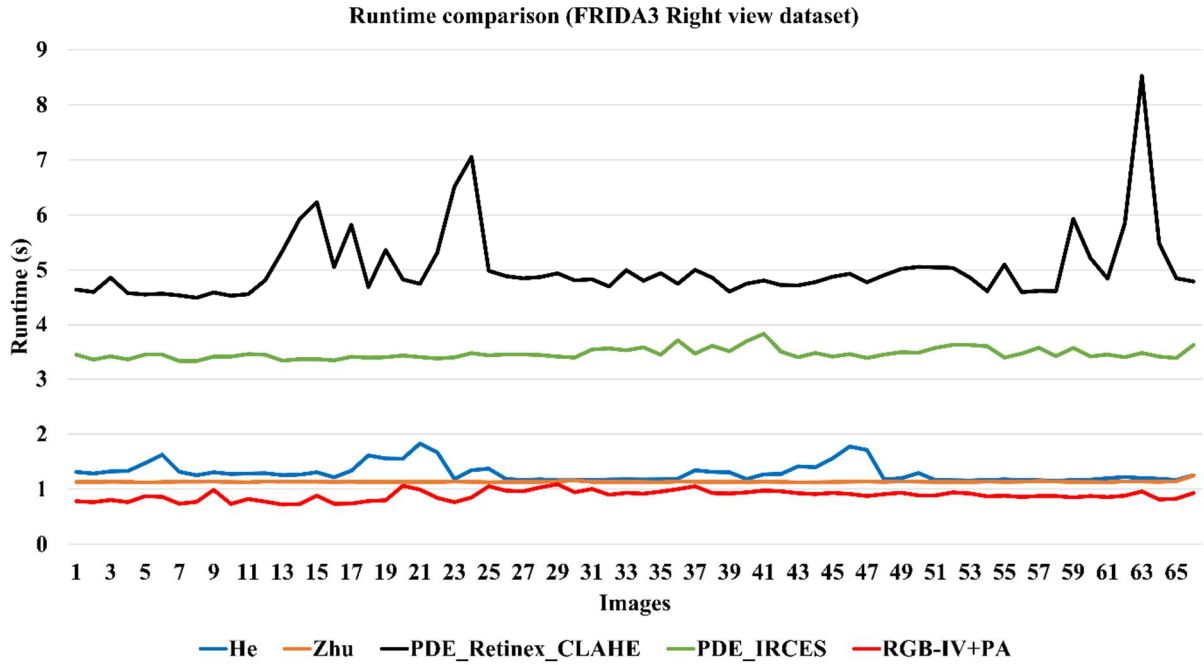

(c)

Figure 7. Runtime comparison of various algorithms using (a) 53 real and 66 synthetic (b) left and (c) right view hazy images

5 Visual comparison of AMEF and PA and Discussion

The key components of the enhancement capability of AMEF are the CLAHE and Gamma Correction (GC) algorithm. Unlike the PDE-GOC-CLAHE, which included the CLAHE and minimized its negative effects [52], the AMEF does not possess such features. We directly compare and present a sample of visual results of the state-of-the-art AMEF with PA in Figs. 8 to 10. Based on visual observation, AMEF generally yields poor results without constant tuning of the clip limit, *c*.

Fig. 8(c) shows that PA can replicate the results of the AMEF by utilizing a high-boost filter with slightly better contrast than AMEF without CLAHE. Adding CLAHE to PA yields better results than AMEF with CLAHE.

The AMEF de-hazing algorithm yields images with halos and colour distortion similar to or worse than the CLAHE- or Retinex-based de-hazing algorithms as seen in the *Brickhouse* image in Fig. 9(b). The AMEF is mainly suited to images with thick haze as seen in the *Train* image in Fig. 9(b), though there is colour fading. The *Horses* images was processed using $c = 0.03$ for AMEF and PA was processed using both filter settings. This is one of the images where AMEF performs adequately, though any slight increase in c leads to heavy colour distortion. Increasing the clip limit of the CLAHE in the AMF leads to increased colour distortion. Additionally, the AMEF algorithm is neither optimized nor adaptive and requires constant tuning of this clip limit parameter to obtain the best results for each hazy image. This makes the AMEF algorithm impractical for effective batch or real-time image de-hazing processing as these issues were consistently observed using several benchmark hazy images. Ultimately, PA is much faster than the AMEF algorithm while yielding good enhancement results without halos, colour degradation or the need to constantly adjust parameters. Also, the AMEF is unable to enhance underwater images, while PA effortlessly performs this operation as seen in Fig. 11.

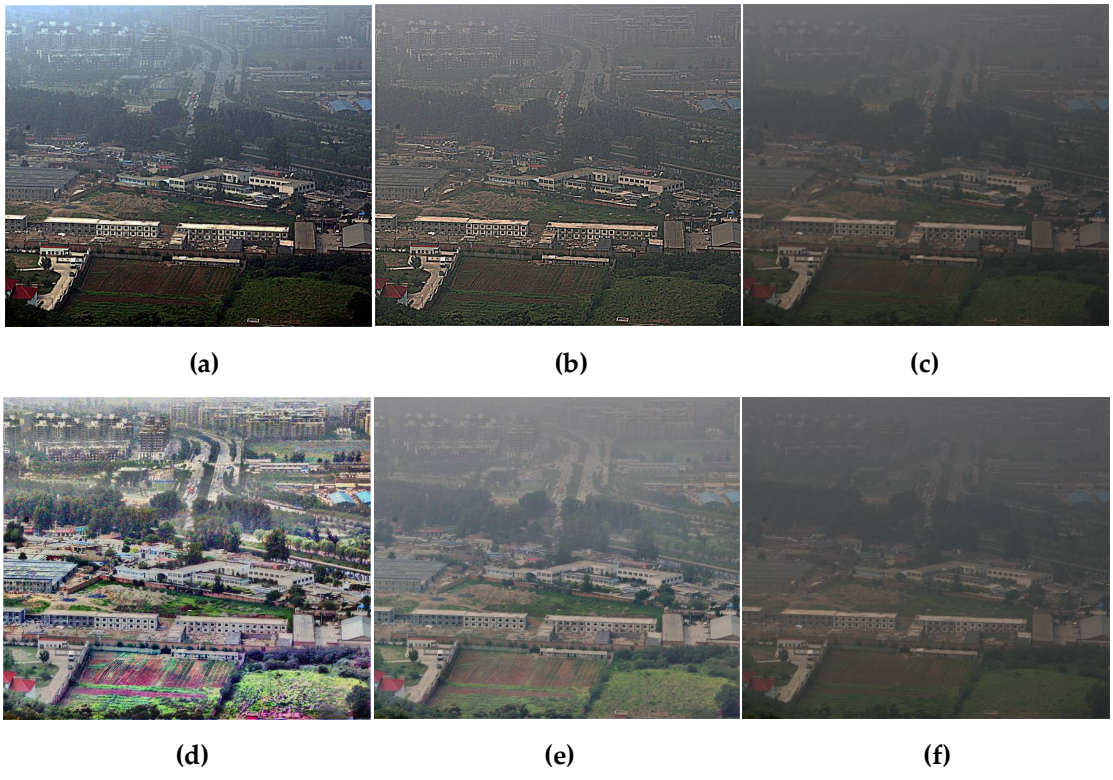

Figure 8. (a) PA (b) without GOCS (c) using high-boost filter setting (d) AMEF ($c = 0.1$) (e) AMEF ($c = 0.01$) (f) AMEF without CLAHE

Peer-reviewed version available at J. Imaging 2018, 4, 108; doi:10.3390/jimaging4090108

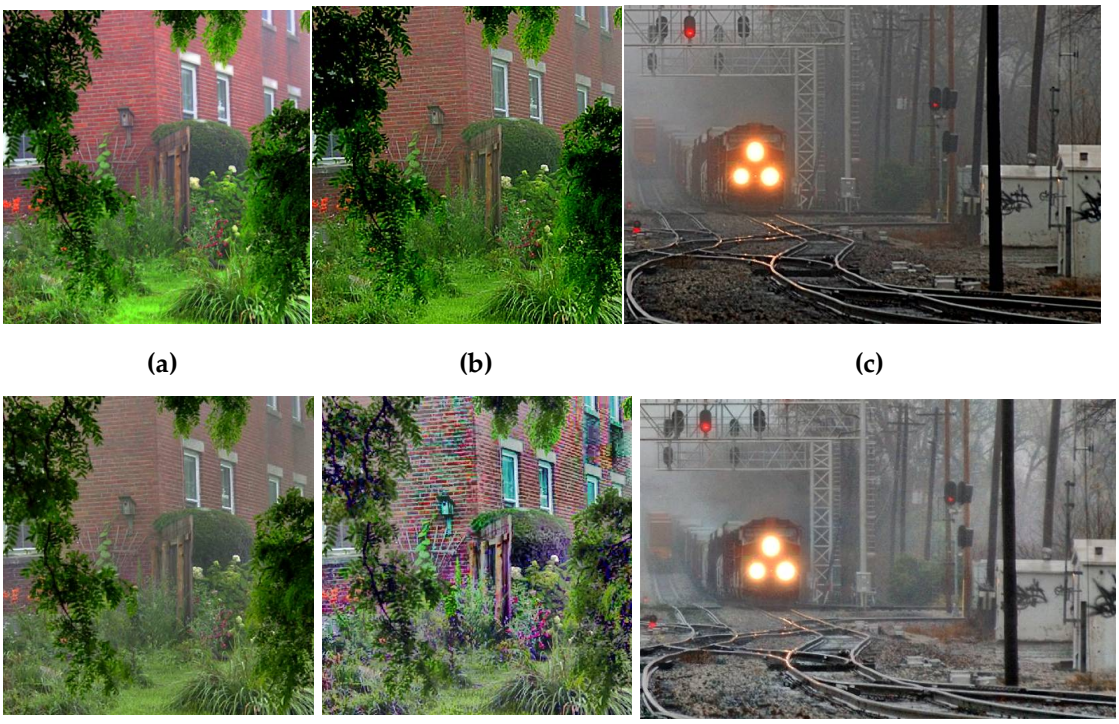

(a) (b) (c)

(d) (e) (f)

Figure 9. (a) PA (high-boost) (b) & (c) PA (d) AMEF (c=0.03) (e) & (f) AMEF (c = 0.1)

(a) (b)

(c) (d)

Figure 10. (a) PA (b) with high-boost filter setting (c) AMEF (c = 0.03) (d) AMEF without CLAHE

Peer-reviewed version available at J. Imaging 2018, 4, 108; doi:10.3390/jimaging4090108

(a) (b) (c)

Figure 11. (a) Original underwater image processed with (b) AMEF (c=0.1) (c) PA

6. Conclusions

A fast, adaptive and versatile multi-scale, fractional order-based hazy and underwater image enhancement algorithm with a relatively simplified structure suitable for hardware implementation has been proposed and developed. The earlier problems of the algorithm were addressed by automated balanced weighting of the filtered images used in the fusion process. The adherence to image entropy and standard deviation features coupled with global and local contrast enhancement ensures that visibility is greatly improved in the final result. Furthermore, comparisons with a recent state-of-the-art multi-scale algorithm shows that the proposed approach is unmatched in several aspects such as speed, consistency, versatility, adaptability and flexibility. Results show that the proposed scheme achieves the stated objectives and can be easily realized in hardware systems for fast image processing in challenging imaging environments.

Funding: This research received no external funding.

Conflicts of Interest: The authors declare no conflict of interest.

References

1. S. Lee, S. Yun, J.-H. Nam, C. S. Won and S.-W. Jung, "A review on dark channel prior based image dehazing algorithms," *EURASIP Journal on Image and Video Processing,* vol. 2016, no. 4, pp. 1-23, 2016.
2. R. Schettini and S. Corchs, "Underwater Image Processing: State of the Art of Smoothing and Image Enhancement Methods," *EURASIP Journal on Advances in Signal Processing,* vol. 2010, pp. 1-14, 2010.
3. K. Gibson and T. Nguyen, "Fast single image fog removal using the adaptive Wiener Filter," in *2013 20th IEEE International Conference on Image Processing (ICIP)*, September 2013.
4. A. Galdran, D. Pardo, A. Picón and A. Alvarez-Gila, "Automatic red-channel underwater image restoration," *Journal of Visual Communication and Image Representation,* vol. 26, pp. 132-145, Jan 31 2015.
5. C. Li, J. Guo, B. Wang, R. Cong, Y. Zhang and J. Wang, "Single underwater image enhancement based on color cast removal and visibility restoration," *Journal of Electronic Imaging,* vol. 25, no. 3, pp. 1-15, June 2016.
6. C. Li and J. Guo, "Underwater image enhancement by dehazing and color correction," *SPIE Journal of Electronic Imaging,* vol. 24, no. 3, p. 033023, 22 June 2015.
7. X. Zhao, T. Jin and S. Qu, "Deriving inherent optical properties from background color and underwater image enhancement," *Ocean Engineering,* vol. 94, pp. 163-172, 2015.
8. J. Chiang and Y. Chen, "Underwater image enhancement by wavelength compensation and dehazing," *IEEE Transactions on Image Processing,* vol. 21, no. 4, pp. 1756-1769, 2012.

9. H. Wen, Y. Tian, T. Huang and W. Gao, "Single underwater image enhancement with a new optical model," in *IEEE International Symposium on Conference on Circuits and Systems (ISCAS)*, May 2013.
10. S. Serikawa and H. Lu, "Underwater image dehazing using joint trilateral filter," *Computers in Elecrical Engineering,* vol. 40, no. 1, pp. 41-50, 2014.
11. N. Carlevaris-Bianco, A. .. Mohan and R. M. Eustice, "Initial results in underwater single image dehazing," in *Proceedings of IEEE International Conference on Oceans*, 2010.
12. J. Y. Chiang, Y.-C. Chen and Y.-F. Chen, "Underwater Image Enhancement: Using Wavelength Compensation and Image Dehazing (WCID)," in *ACIVS 2011, LNCS 6915*, 2011.
13. K. Iqbal, R. A. Salam, A. Osman and A. Z. Talib, "Underwater image enhancement using an integrated color model," *IAENG International Journal of Computer Science,* vol. 34, no. 2, pp. 529-534, January 2007.
14. A. S. A. Ghani and N. A. M. Isa, "Underwater image quality enhancement through integrated color model with Rayleigh distribution," *Applied Soft Computing,* vol. 27, pp. 219-230, 2015.
15. X. Fu, P. Zhuang, Y. Huang, Y. Liao, X.-P. Zhang and X. Ding, "A retinex-based enhancing approach for single underwater image," in *Proceedings of International Conference on Image Processing (ICIP)*, 27 October 2014.
16. H. Gouinaud, Y. Gavet, J. Debayle and J.-C. Pinoli, "Color Correction in the Framework of Color Logarithmic Image Processing," in *IEEE 7th International Symposium on Image and Signal Processing and Analysis (ISPA 2011)*, Dubrovnik, Croatia, Sep 2011.
17. S. Bazeille, I. Quidu, L. Jaulin and J. P. Malkasse, "Automatic underwater image pre-processing," in *Proceedings of the Characterisation du Milieu Marin (CMM '06)*, 2006.
18. M. Chambah, D. Semani, A. Renouf, P. Coutellemont and A. Rizzi, "Underwater Color Constancy : Enhancement of Automatic Live Fish Recognition," in *16th Annual symposium on Electronic Imaging*, Inconnue, United States, 2004.
19. L. A. Torres-Mendez and G. Dudek, "Color correction of underwater images for aquatic robot inspection," in *Proceedings of the 5th International Workshop on Energy Minimization Methods in Computer Vision and Pattern Recognition (EMMCVPR '05)*, Augustine, Fla, USA, November 2005.
20. J. Ahlen, D. Sundgren and E. Bengtsson, "Application of underwater hyperspectral data for color correction purposes," *Pattern Recognition and Image Analysis,* vol. 17, no. 1, p. 170–173, 2007.
21. J. Ahlen, Colour correction of underwater images using spectral data, Uppsala University, 2005.
22. F. Petit, A.-S. Capelle-Laizé and P. Carré, "Underwater image enhancement by attenuation inversion with quaternions," in *Proceedings of the IEEE International Conference on Acoustics, Speech and Signal Processing (ICASSP '09)*, Taiwan, 2009.
23. G. Bianco, M. Muzzupappa, F. Bruno, R. Garcia and L. Neumann, "A New Colour Correction Method For Underwater Imaging," *The International Archives of the Photogrammetry, Remote Sensing and Spatial Information Sciences Underwater 3D Recording and Modeling,* Vols. XL-5/W5, no. 5, Piano di Sorrento, Italy, pp. 25-32, 16–17 April 2015.
24. C. Prabhakar and P. K. Praveen, "An Image Based Technique for Enhancement of Underwater Images," *International Journal of Machine Intelligence,* vol. 3, no. 4, pp. 217-224, 2011.
25. H. Lu, Y. Li, L. Zhang and S. Serikawa, "Contrast enhancement for images in turbid water," *Journal of Optical Society of America,* vol. 32, no. 5, pp. 886-893, May 1 2015.

26. U. A. Nnolim, "Smoothing and enhancement algorithms for underwater images based on partial differential equations," *SPIE Journal of Electronic Imaging,* vol. 26, no. 2, pp. 1-21, March 22 2017.
27. U. A. Nnolim, "Improved partial differential equation (PDE)-based enhancement for underwater images using local-global contrast operators and fuzzy homomorphic processes," *IET Image Processing,* vol. 11, no. 11, pp. 1059-1067, November 2017.
28. R. Garcia, T. Nicosevici and X. Cufi, "On the way to solve lighting problems in underwater imaging," in *Proceedings of the IEEE Oceans Conference Record*, 2002.
29. Y. Rzhanov, L. M. Linnett and R. Forbes, "Underwater video mosaicing for seabed mapping," in *Proceedings of IEEE International Conference on Image Processing*, 2000.
30. H. Singh, J. Howland, D. Yoerger and L. Whitcomb, "Quantitative photomosaicing of underwater imaging," in *Proceedings of the IEEE Oceans Conference*, 1998.
31. R. Fattal, "Dehazing using Colour Lines," *ACM Transactions on Graphics,* vol. 28, no. 4, pp. 1-14, August 2009.
32. K. He, J. Sun and X. Tang, "Single Image Haze Removal Using Dark Channel Prior," *IEEE Transactions on Pattern Analysis and Machine Intelligence (PAMI),* vol. 33, no. 12, pp. 2341-2353, 2010.
33. S. Fang, J. Zhan, Y. Cao and R. Rao, "Improved single image dehazing using segmentation," in *17th IEEE International Conference on Image Processing (ICIP)*, 26-29 Sept. 2010.
34. T. Cui, J. Tian, E. Wang and Y. Tang, "Single image dehazing by latent region-segmentation based transmission estimation and weighted L1-norm regularisation," *IET Image Processing* , vol. 11, no. 2, pp. 145-154, Jan. 16 2017.
35. V. Senthamilarasu, A. Baskaran and K. Kutty, "A New Approach for Removing Haze from Images," in *Proceedings of the International Conference on Image Processing, Computer Vision, and Pattern Recognition (IPCV)*, The Steering Committee of The World Congress in Computer Science, Computer Engineering and Applied Computing (WorldComp)., Jan 1, 2014.
36. C. O. Ancuti, C. Ancuti and P. Bekaert, "Effective single image dehazing by fusion," in *17th IEEE International Conference on Image Processing (ICIP)*, 26-29 Sept. 2010.
37. A. Galdran, J. Vazquez-Corral, D. Pardo and M. Bertalmıo, "Fusion-based Variational Image Dehazing," *IEEE Signal Processing Letters,* vol. 24, no. 2, pp. 151-155, Feb 2017.
38. P. Carr and R. Hartley, "Improved Single Image Dehazing using Geometry," in *IEEE Digital Image Computing: Techniques and Applications, 2009. DICTA'09.* , Dec. 1, 2009 .
39. D. Park, D. K. Han and H. Ko, "Single image haze removal with WLS-based edge-preserving smoothing filter," in *IEEE International Conference on Acoustics, Speech and Signal Processing (ICASSP)*, 26-31 May 2013.
40. A. Galdran, J. Vazquez-Corral, D. Pardo and M. Bertalmio, "A Variational Framework for Single Image Dehazing," September 2014.
41. A. Galdran, J. Vazquez-Corral, D. Pardo and M. Bertalmio, "Enhanced Variational Image Dehazing," *SIAM Journal on Imaging Sciences,* pp. 1-26, September 2015.
42. X. Liu, F. Zeng, Z. Huang and Y. Ji, "Single color image dehazing based on digital total variation filter with color transfer," in *20th IEEE International Conference on Image Processing (ICIP)*, 15-18 Sept. 2013.
43. X.-M. Dong, X.-Y. Hu, S.-L. Peng and D.-C. Wang, "Single color image dehazing using sparse priors," in *17th IEEE International Conference on Image Processing (ICIP)*, 26-29 Sept. 2010.

44. G. Meng, Y. Wang, J. Duan, S. Xiang and C. Pan, "Efficient Image Dehazing with Boundary Constraint and Contextual Regularization," in *IEEE International Conference on Computer Vision (ICCV-2013)*, 2013.

45. X.-S. Zhang, S.-B. Gao, C.-Y. Li and Y.-J. Li, "A Retina Inspired Model for Enhancing Visibility of Hazy Images," *Frontiers in Computer Science,* vol. 9, no. 151, pp. 1-13, 22nd December 2015.

46. W. Ren, S. Liu, H. Zhang, J. Pan, X. Cao and M.-H. Yang, "Single Image Dehazing via Multi-Scale Convolutional Neural Networks," in *European Conference on Computer Vision* , Springer International Publishing, Oct. 8, 2016 .

47. S. Yang, Q. Zhu, J. Wang, D. Wu and Y. Xie, "An Improved Single Image Haze Removal Algorithm Based on Dark Channel Prior and Histogram Specification," in *3rd International Conference on Multimedia Technology (ICMT-13)*, Nov. 22, 2013.

48. F. Guo, Z. Cai, B. Xie and J. Tang, "Automatic Image Haze Removal Based on Luminance Component," in *6th International Conference on Wireless Communications Networking and Mobile Computing (WiCOM)*, 23-25 Sept. 2010.

49. D. Nair, P. A. Kumar and P. Sankaran, "An Effective Surround Filter for Image Dehazing," in *ICONIAAC '14*, Amritapuri, India, October 10 - 11 2014.

50. B. Xie, F. Guo and Z. Cai, "Improved Single Image Dehazing Using Dark Channel Prior and Multi-scale Retinex," in *International Conference on Intelligent System Design and Engineering Application (ISDEA)*, 13-14 Oct. 2010.

51. U. A. Nnolim, "Sky detection and log illumination refinement for PDE-based hazy image contrast enhancement," 2017. [Online]. Available: http://arxiv.org/pdf/1712.09775.pdf. [Accessed December 2017].

52. U. A. Nnolim, "Partial differential equation-based hazy image contrast enhancement," *Computers and Electrical Engineering,* vol. (in print), pp. 1-11, February 21 2018.

53. U. A. Nnolim, "Image de-hazing via gradient optimized adaptive forward-reverse flow-based partial differential equation," *Journal of Circuits Systems and Computers,* (accepted), pp. 1-35, July 5 2018.

54. A. Galdran, "Artificial Multiple Exposure Image Dehazing," *Signal Processing,* vol. 149, pp. 135-147, August 2018.

55. Q. Yang, D. Chen, T. Zhao and Y. Chen, "Fractional calculus in image processing: a review," *Fractional Calculus and Applied Analysis,* vol. 19, no. 5, pp. 1222-1249, Oct 1 2016 .

56. V. Patrascu, "Image enhancement method using piecewise linear transforms," in *European Signal Processing Conference (EUSIPCO-2004)*, Vienna, Austria, 2004.

57. A. B. Baliga, "Face Illumination Normalization with Shadow Consideration," Masters Thesis, Department Of Electrical and Computer Engineering, Carnegie Mellon University, Pittsburgh, May 2004.

58. U. A. Nnolim, "An adaptive RGB colour enhancement formulation for Logarithmic Image Processing-based algorithms," *Optik* , vol. 154 , p. 192–215, February 2018.

59. X. Shen, Q. Li, Y. Tan and L. Shen, "An Uneven Illumination Correction Algorithm for Optical Remote Sensing Images Covered with Thin Clouds," *Remote Sensing,* vol. 7, no. 9, pp. 11848 - 11862, September 2015.

60. K. Matkovic, L. Neumann, A. Neumann, T. Psik and W. Purgathofer, "Global Contrast Factor-a New Approach to Image Contrast," in *Proceedings of the 1st Eurographics Conference on Computational Aesthetics in Graphics, Visualization and Imaging*, Girona, Spain, May 18-20, 2005.

61. S. Susstrunk and D. Hasler, "Measuring Colourfulness in Natural Images," in *IS&T/SPIE Electronic Imaging 2003: Human Vision and Electronic Imaging VIII*, 2003.
62. C. Ancuti, C. Ancuti, T. Haber and P. Bekaert, "Enhancing underwater images and videos by fusion," in *IEEE Conference on Computer Vision and Pattern Recognition*, Jun 16 2012.
63. L. Caraffa and J.-P. Tarel, "Stereo Reconstruction and Contrast Restoration in Daytime Fog," in *11th IEEE Asian Conference on Computer Vision (ACCV'12), part 4*, Daejeon, Korea, November 2012.
64. J.-P. Tarel, A. Cord, H. Halmaoui, D. Gruyer and N. Hautiere, "FRIDA3 image database," 2012.
65. J. Tarel and N. Hautiere, "Fast visibility restoration from a single color or gray level image," in *IEEE 12th International Conference on Computer Vision*, Sep 2009.
66. S.-k. Dai and J.-P. Tarel, "Adaptive Sky Detection and Preservation in Dehazing Algorithm," in *IEEE International Symposium on Intelligent Signal Processing and Communication Systems (ISPACS)*, November 2015.
67. K. Nishino, L. Kratz and S. Lombardi, "Bayesian Defogging," *International Journal of Computer Vision*, vol. 98, no. 3, p. 263–278, July 2012.
68. W. Wang and C. He, "Depth and Reflection Total Variation for Single Image Dehazing," Chongqing, China, October 2016.
69. Q. Zhu, J. Mai and L. Shao, "A Fast Single Image Haze Removal Algorithm Using Color Attenuation Prior," *IEEE Transactions on Image Processing*, vol. 24, no. 11, pp. 3522-3533, November 2015.

544
545